Self-assembled gold decorated polydopamine nanospheres as electrochemical sensor for simultaneous determination of ascorbic acid, dopamine, uric acid and tryptophan

Andrés Arroquia, Irene Acosta, M. Pilar García Armada

Self-assembled gold decorated polydopamine nanospheres as electrochemical sensor for simultaneous determination of ascorbic acid, dopamine, uric acid and tryptophan.

Andrés Arroquia, Irene Acosta, M. Pilar García Armada*

Department of Industrial Chemical Engineering, Escuela Técnica Superior de Ingenieros Industriales, Universidad Politécnica de Madrid, José Gutierrez Abascal, 2, Madrid 28006, Spain.

Corresponding autor: M. Pilar García Armada, ORCID: 0000-0003-2410-3365; pilar.garcia.armada@upm.es

Declarations of interest: none

Self-assembled gold decorated polydopamine nanospheres as electrochemical sensor for simultaneous determination of ascorbic acid, dopamine, uric acid and tryptophan.

Andrés Arroquia, Irene Acosta, M. Pilar García Armada*
Department of Industrial Chemical Engineering, Escuela Técnica Superior de Ingenieros Industriales, Universidad Politécnica de Madrid, José Gutierrez Abascal, 2, Madrid 28006, Spain.

Corresponding autor: M. Pilar García Armada, ORCID: 0000-0003-2410-3365; pilar.garcia.armada@upm.es

Abstract

Herein, a new sensor based on screen-printed carbon electrodes covalently modified with self-assembled gold-decorated-polydopamine nanospheres (Au-PDNs) is reported. The sensor was applied to the simultaneous determination of the biologically significant molecules ascorbic acid (AA), dopamine (DA), uric acid (UA) and tryptophan (TR). The Au-PDNs were anchored to gold nanoparticles electrodeposited onto the bare electrodes via cysteamine-glutaraldehyde bridges, and were characterized by scanning and transmission electron microscopies. The stepwise fabrication of the electrodes and their electrochemical responses were evaluated by cyclic voltammetry, electrochemical impedance spectroscopy and differential pulse voltammetry. The response of the new device to these analytes is pH-dependent, which allows selecting the best working conditions as a function of the sample characteristics. At pH values of 3.0 and 8.0, it was possible to determine simultaneously AA, UA and TR in presence of DA, and DA, UA and TR in presence of AA respectively, with very wide linear ranges and high sensitivities. The simultaneous determination of AA, DA, UA and TR was possible at pH 6.0 with competitive sensitivities in two consecutive linear ranges, between 10 – 80 μM and 80 – 240 μM; 1 – 160 μM and 160 – 350 μM; 10 – 120 μM and 120 – 350 μM; and 1 – 160 μM and 160 – 280 μM, respectively. The obtained limits of detection were 0.2 nM, 0.1 nM, 0.1 nM and 0.1 nM, respectively.

Keywords Polydopamine nanospheres; Self-assambled monolayer; Ascorbic acid; Dopamine; Uric acid; Triptophan;

1. Introduction

The research on determination of biologically interesting molecules is an open field in continuous symbiotic development together with the biomedical sciences. The early diagnosis of diseases requires increasingly sensitive and selective analytical methods for the biomolecules of interest. Ascorbic acid (AA) is an essential vitamin in the human nutrition and a common antioxidant in the diet. AA plays an important role in the synthesis of the triple collagen helix and its absence or excess cause several diseases such as scurvy or nephrolithiasis [1,2]. Uric Acid (UA) is the primary final product of the purines metabolism in humans and abnormal levels in blood or urine cause diseases as hyperuricemia or gout [3,4]. Dopamine (DA) is an important neurotransmitter in the mammalian central nervous system, which deficiency is related to several mental illnesses such as psychosis or Parkinson's disease [5,6]. Tryptophan (TR) is an essential amino acid, involved in the establishment and maintenance of the positive nitrogen balance, and precursor of neurotransmitters and hormones as serotonin, melatonin, dopamine or epinephrine. Low TR levels are associated with stress, depression, and even schizophrenia [7,8]. These molecules have similar structures and usually coexist in the biological samples, causing cross interferences in its respective determinations. The determination of each one of these molecules requires the elimination of interfering substances by physical or chemical separation, or the determination of all of them. For this reason, the majority of reported determination methods pursuit the simultaneous determination of the largest possible number of sample components, and the development of improved, fast, sensitive and selective methods remains a significant research objective [9].

Due to the redox properties of these molecules, the electrochemical techniques have obtained great attention because its low cost, simple operation and rapid response, in comparison with chromatography [10]. However, the sensitivity and low detection limits achieved until now seems to be insufficient to detect the common levels of some analytes in the biological fluids [11]. Taking into account that, at conventional electrodes, the AA, DA UA and TR oxidation occurs at very close potentials, overlapping the electrochemical signals, the most widely used method is the differential pulse voltammetry (DPV) with modified electrodes. This technique provides good peaks' resolution and low detection levels. These facts have motivated the developing of a lot of modified electrodes for the individual or simultaneous determination of these biomolecules, with materials as carbon paste [12], polymers [13,14], dendrimers [15], metallic nanoparticles [16-19] to carbon nanotubes [20-22] or graphene [23,24]. Many of these sensors undergo an important fouling effect due to adsorption of the oxidation products that cause poor reproducibility [25]. The properties of all these devices, as linear ranges, sensitivity and limits of detection, continue to improve as new materials and electrode designs are developed. Another important aspect, according to a recent review [26] would be to advance towards the on-site analyses of biologically important compounds, in order to allow their determination without going to a hospital.

Polydopamine (PDA) is an interesting biocompatible polymer that has been used as universal surfaces modification agent to develop applications in fields as different as biotechnology [27], electrochemical sensing [28,29] or nanotechnology applied to development of batteries [30]. PDA is the final product of the spontaneous oxidation of dopamine, in aqueous solutions, with oxygen [31] and it is able to form nanospheres (PDNs) in stirred alkaline media [32]. In the last years, some strategies based on the control of the reaction pH, temperature or dopamine concentration have been developed in order to prepare monodisperse size-controlled colloidal PDNs [33,34]. Particularly, the pH of the reaction has a critical influence on the reaction rate and number of nuclei

formed, and thus on the nanospheres size. These PDNs have been used as biocompatible filler for a new-generation of multifunctional biocomposites [35], as photothermal therapeutic agents [36,37], as anti-cancer drug delivery [38,39] and other applications [40]. An important feature of the PDNs surface is the high density of catechol and amine functional groups [41], which are able to reduce the metallic ions to form in-situ metallic nanoparticles uniformly distributed on the polymer film [29,42,43]. These composites have been used as catalysts [44,45], as synergetic chemo-photothermal cancer therapy [46] and other applications [47-50].

Gold nanoparticles (AuNPs) are the most frequently used nanomaterial because their excellent size-dependent optical and electronic properties, chemical stability and high surface area. AuNPs and their hybrids have been successfully and widely applied in the nanoscience and nanotechnology fields [51], and principally as catalysts in the development of sensors [52] and biosensors [53,54]. The modification of PDA with gold nanoparticles extends the PDNs applications due to the electro chemical properties-biocompatibility synergic effect [28,55, 56]. In addition, in the case of PDNs, the modification with AuNPs also improves its chemical stability [28]. The good conductivity of PDA, PDNs and Au-PDNs [42] makes them suitable for developing ultrasensitive electrochemical immunosensors [42], sensors and biosensors [28,55,56].

The PDNs attracted our attention by its easy synthesis, its possibilities of size control and because its functional groups can be anchored to other structures and supports through a covalent bond [41,36-38]. In this way, it is possible to extend its functionalities forming conjugates, including the formation of self-assembled monolayers (SAMs), for sensing applications. The self-assembly technique [39] is widely employed in the development of sensors and biosensors [57-59]. SAMs formed by thiols on gold electrodes are stable and well-organized and show good selectivity, sensitivity, short response-time and small overpotential in electrocatalytic reactions [60-62].

Herein, we report a new electrochemical sensor for the simultaneous determination of AA, DA, UA and TR based on SAMs formed by Au-PDNs covalently bonded to an AuNPs layer via cysteamine-glutaraldehyde bonds. This structure is chemically stable, electrically conductive, easily reproducible, and maintains all the Au-PDNs properties. We are convinced that the on-site analyses of biologically important compounds is a significant target and, therefore, a reusable glassy carbon and two kinds of screen-printed carbon electrodes, all covered with electrodeposited AuNPs, were used in order to develop a portable sensor for low volumes of sample and measurements *in situ*, with lower costs and simple analysis process. The report includes the morphological, electrochemical and analytical characterization of sensors.

2. Material and methods

2.1. Reagents and solutions

Ascorbic acid, dopamine hydrochloride, chloroauric acid, L-ascobic acid, uric acid, folic acid, glucose, cysteamine and glutaraldehyde were purchased from Sigma-Aldrich. Trichloroacetic acid, potassium chloride and L-tryptophan were supplied by Fluka chemika. Phosphate buffer saline solutions (PBS) 0.1 M at several pH values were prepared using 0.1 M KCl, 0.1 M Na_2HPO_4, 0.1 M KH_2PO_4 and H_3PO_4. All other chemicals were used in analytical grade without furthers purifications. Ultrapure water was used for preparation of buffers and standards, and for the electrochemistry solutions. The gold nanoparticles layer was electrodeposited from an aqueous solution containing

$HAuCl_4$ 0.1 mM and trichloroacetic acid 50 mM. The solutions were deoxygenated by bubbling high-purity nitrogen for at least 15 min prior to the electrochemical measurements.

2.2. Apparatus

All the electrochemical measurements were performed using an Ecochemie BV Autolab PGSTAT 12. The experiments were carried out in a conventional three-electrode cell at 20–21 ◦C with a saturated calomel reference electrode (SCE), a Pt wire as auxiliary and a 3 mm diameter glassy carbon disc (GC), a carbon screen-printed DropSens DRP-C110 (C_{110}) (4 mm diameter), or a carbon nanostructured screen-printed Orion OHT C101 (C_{101}) (4 mm diameter) as working electrodes. The electrochemical impedance spectroscopy (EIS) measurements were carried out at 0.2 V vs. Ag/AgCl electrode, over the frequency range of 0.1 to 10000 Hz, with 10 mV AC perturbation, in a 10 mM $K_3Fe(CN)_6/K_4Fe(CN)_6$ (1:1) solution containing 0.1 M KCl. The transmission electron microscopy (TEM) images were obtained using a JEOL JEM 2100, with a resolution of 0.25 nm, voltage acceleration of 200 kV and energy-dispersive X-ray spectroscopy system (EDS). The scanning electron microscopy (SEM) images were obtained with a JEOL JSM 6400. For the DPV studies, a scan rate of 55.5 mV s^{-1}, pulse time of 30 ms and pulse amplitude of 40 mV were used. The DPV determinations were carried out by the standard addition method.

2.3. PDNS synthesis

Although a certain relation between the PDNs diameter and the hydroxide concentration has been reported [34], only sizes of 20 nm, 196 nm and 367 nm have been previosly prepared. In order to prove if a wider correlation can be inferred from this work, we have taken a polynomial fit to intra- and extrapolate the hydroxide concentrations (y, $mM = 4 \cdot 10^{-5}x^2 - 0.0391x + 11.324$, being x the PDNS diameter in nm) as hypothesis, and we have thus synthesized the PDNS by procedures based on the previously described methods [32,34]. Briefly, the adequate quantities of NaOH solution were added to respective 10.5 mM dopamine hydrochloride aqueous stirred solutions until reaching concentrations of 2.00 mM and 6.00 mM of NaOH. The mixture was allowed to react for 3 hours under stirring at 50ºC. The colour of the solution turned firstly to pale yellow and finally to dark brown. Finally, the PDNs were separed by centrifugation (12000 rpm) and washed with ultrapure water. The PDNs were dried and stored at 4 ºC.

2.4. Au-PDNS preparation

The obtained PDNs suspension was mixed with a 1 mM $HAuCl_4$ solution, and then 0.5 mM ascorbic acid was added to the mixture as reductor. The reaction was maintained during 3 hours at 30ºC with stirring [28]. The suspension turns gradually from dark brown to dark purple (Fig. S1). Finally, the Au-PDNs were separed by centrifugation and washed with water. The Au-PDNs were dried and stored in the dark at 4 ºC.

2.5. Electrodes preparation

Prior to use, GCE was polished successively with 3.0 and 0.05 μm alumina powder, rinsed thoroughly with ultrapure water and sonicated after each step. Finally, the electrode was dried at room temperature. C_{110} and C_{101} screen-printed electrodes were used as it. Fig. 1 shows the scheme followed to prepare the modified electrodes.

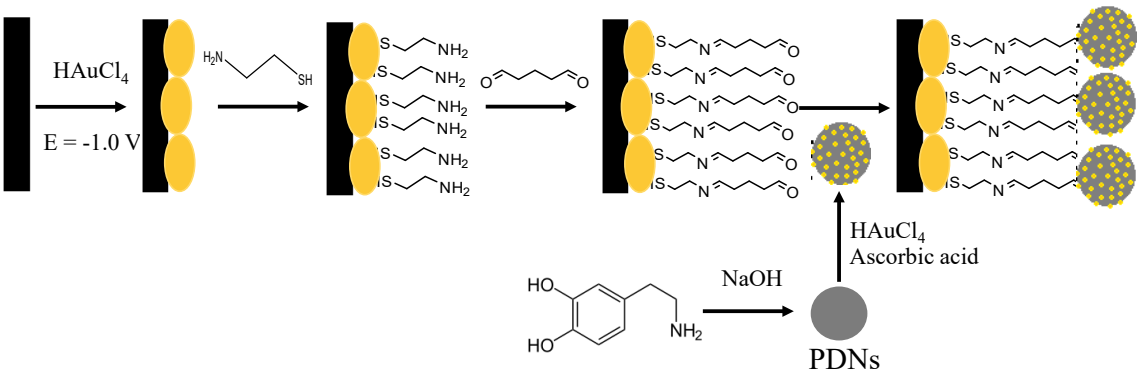

Fig. 1. Electrode preparation scheme

To form the anchor layer on carbon electrodes, AuNPs were electrodeposited under potentiostatic control at -1 V *vs.* SCE, during 300 s, and washed with ultrapure water [63]. The second layer was formed by dipping the modified electrodes in a 0.1M cysteamine solution for 3 h to form the Au-S bonds and functionalize the electrodes with amine terminal groups, followed by washing with water. In order to form the covalent bonds between the modified electrode and the surficial amine groups of the PDNs and get the cysteamine chains longer, the bi-functional reactant glutaraldehyde was used. Therefore, the third self-assembled layer was built by dipping the modified electrodes in a 25% glutaraldehyde solution for 3 hours and then rinsed with water. In order to form the last layer, 8 µl of the aqueous suspension of Au-PDNs (0.2 mg mL^{-1}) of corresponding size were dropped on the above prepared surfaces and remained for 3 hours at room temperature in the dark. Finally, the electrodes were washed with water, dried, and stored in the dark at room temperature when not in use.

3. Results and discussion

3.1. Characterization of PDNs and Au-PDNs

The morphology of synthesized PDNs and Au-PDNs was characterized by TEM (Fig. 2). As it can be seen, the smaller PDNs (Fig. 2a) appear well dispersed with sizes close to 150 nm, while the bigger PDNs (Fig. 2b) show a larger size dispersion, with an 80 % of them in the range of 470±40 nm and maximum size of 570 nm. These findings confirm the initial hypothesis, with little variation in the polynomial fit (Fig. S2). Fig. 2c also shows the result of the AuNPs modification of PDNs (470 nm as an example). As it can be seen, little AuNPs (about 6-7 nm) cover the PDNs surface, in agreement with previous reports [28], but also, the TEM image let us know that a lot of greater AuNPs (about 30 nm) have formed within the nanosphere. This fact have not been reported up to now and it is currently on study. The formation of inner AuNPs causes a light increase in the size of Au-PDNS in comparison with the initial PDNs, especially in the smaller PDNs. The energy-dispersive-X-ray spectroscopy (EDS) of the PDNs and Au-PDNs (Fig. S3) confirms the existence of only C, H and O, and C, H, O and Au respectively.

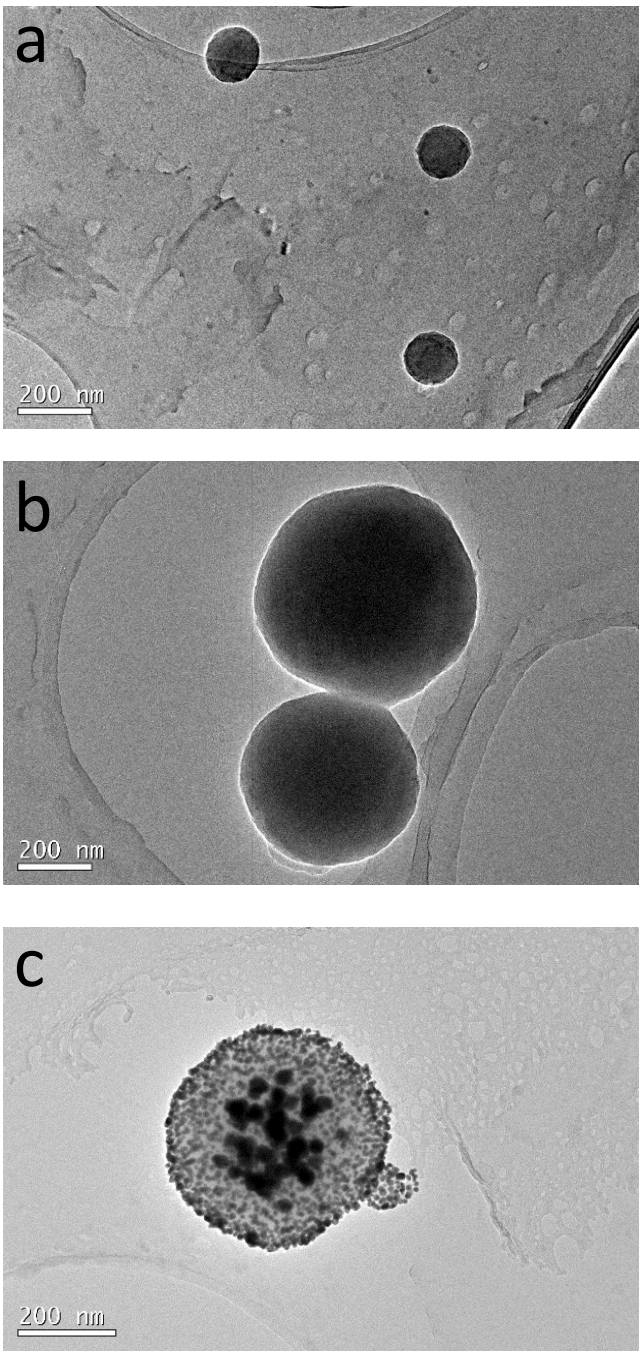

Fig. 2. TEM images of the obtained PDNs with diameters of 150 nm (a) and 470 nm (b) and of the obtained Au-PDNs from the 470 PDNS (c).

3.2. Characterization of modified electrodes

The formation of the self-assembled layer was studied in PBS 0.1M (pH 7) by cyclic voltammetry using GC and C_{110} as bare electrodes. Fig. 3 shows the steady state CVs of the several steps of the electrodes' modification. As can be seen, the background signals of both AuNPs/GC (Fig. 6a) and AuNPs/C_{110} (Fig. 3b) electrodes increases as result from the larger effective surface area of AuNPs. After the electrodeposition of AuNPs, both

voltammograms clearly show the typical oxide formation and reduction on their surface. Fig. 3a shows the asymmetric and narrow irreversible redox system of cysteamine at 0.6 and 0.0 V [64].

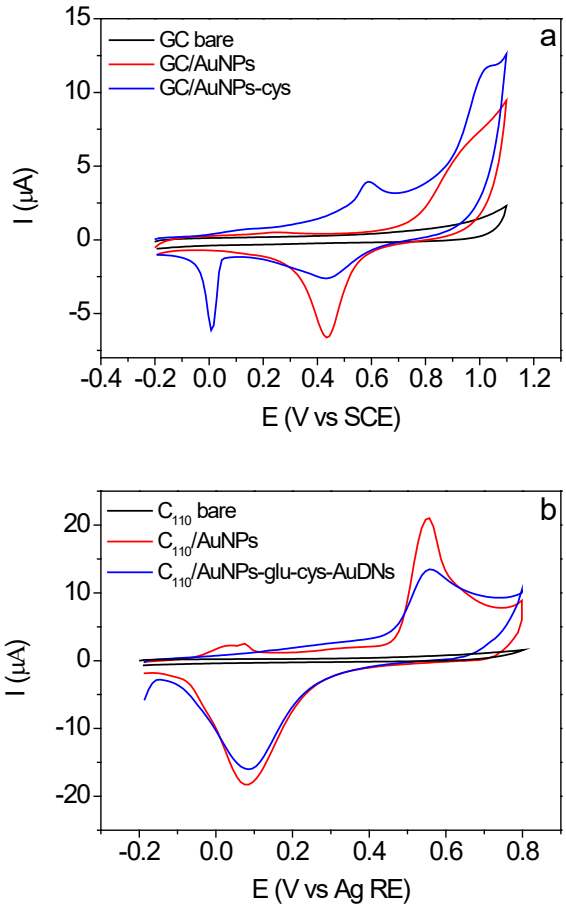

Fig. 3. Voltammetric responses of (a) bare GCE, GCE/AuNPs and GCE/AuNPs-cys and (b) bare C_{110}, C_{110}/AuNPs and C_{110}/AuNPs-cys-glu-Au-PDNs (C_{110}-sensor), all in PBS 0.1M (pH 7). Scan rate 20mV/s.

The intensity of these peaks falls during the second and successive scans, and disappears from the 30th scan (not shown), suggesting the cysteamine desorption from the Au surface. Other authors [61] earlier observed this fact in alkaline solution concluding that voltammetric scans to negative potentials reduces irreversibly the Au-S bond, liberating the thiol containing molecules according to:

$$\text{Support-AuNPs-glu=N-(CH}_2\text{)}_2\text{-S-Au} + e^- \rightarrow \text{Au} + \text{Support-AuNPs-glu =N-(CH}_2\text{)}_2\text{-S}^-$$

It seems clear that the covalently bounded cysteamine is also reductively desorbed in PBS (pH 7.0) and, although in this case some re-adsorption occurs at 0.6 V, the scan to the cysteamine reduction potential must be avoided. Fig. 3b shows the CV obtained with a completely modified C_{110}/AuNPs-cys-glu-Au-PDNs electrode (C_{110}-sensor) to be compared with the bare and C_{110}/AuNPs electrodes. As it can be seen, the oxide formation and reduction in the gold surface is practically recovered after the AuDNS modification of the insulating glutaraldehyde layer [26]. The final gold effective area is rather smaller than C_{110}/AuNPs electrode because the AuNPs-anchor are now functionalized and the PDNs' AuNPs are small and uniformly distributed.

The GC-, C_{110}- and C_{101}-sensors were also characterized by cyclic voltammetry in 0.1 M KCl containing 1.0 mM $K_3[Fe(CN)_6]$, as a benchmark redox reaction for modified electrodes (Fig. 4).

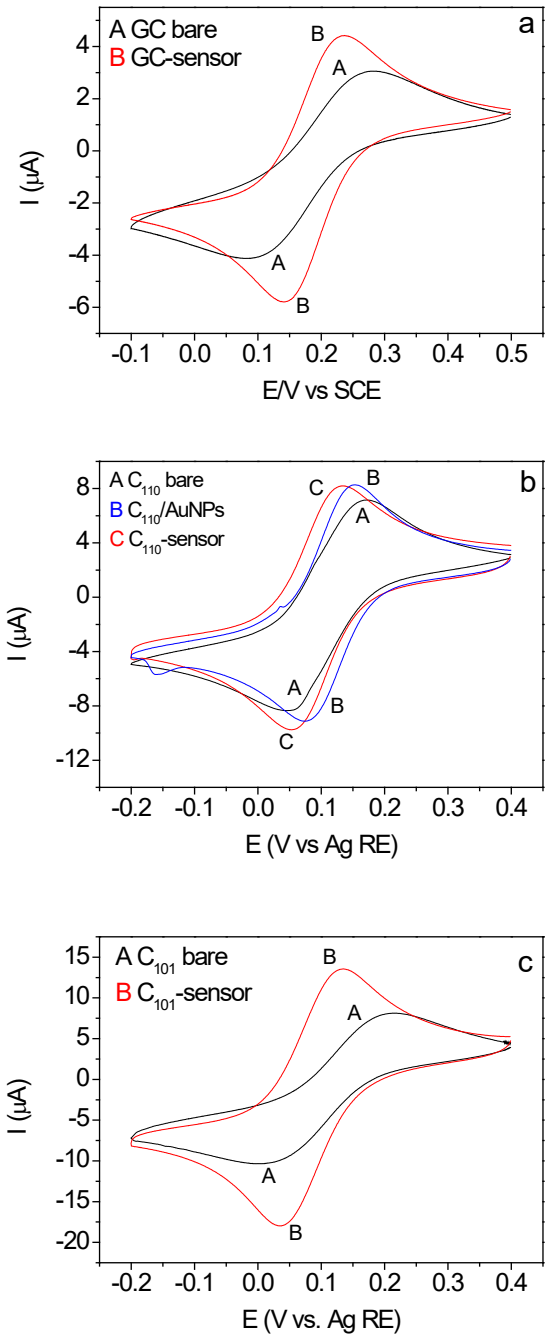

Fig. 4. CVs at GC (a), C_{110} (b) and C_{101} (c), bare and totally modified electrodes, in 0.1 M KCl containing 1.0 mM $K_3[Fe(CN)_6]$. Scan rate 20 mV/s. Figure (b) also shows the C_{110}/AuNPs in the same conditions.

As expected, the bare GC shows the lowest peak current. In all cases, the sensors show higher peak current than the bare electrodes, indicating good conductivity. Fig. 4b also shows the voltammetric response at the intermediate step C_{110}/AuNPs. The increases in the peaks currents and the peak potential narrow difference after the SAM formation, even in comparison with the AuNPs (Fig. 4b), indicates a fast electron transfer process.

The active surface areas of the three type of sensors (bare as well as modified) were calculated from the Randles-Sevcic equation, [65,66]:

$$I_p = 2.69 \cdot 10^5 \, A \, D^{1/2} \, n^{3/2} \, v^{1/2} \, C$$

where n is the number of transferred electrons, A is the active surface area, D is the diffusion coefficient of $K_3[Fe(CN)_6]$, $6.7 \cdot 10^{-6}$ cm^2/s [66], v is the scan rate (V/s), and C is the concentration of analyte (mol/cm^3). The increases of active surface areas obtained for the CG-, C_{110}- and C_{101}-sensors in relation with the bare electrodes were 31.6 %, 28.0 % and 68.4 %, demonstrating the higher electrochemical activity of the modified electrodes, mainly the nanostructured C_{101}.

The morphology of sensors was studied by scanning electron microscopy (SEM). Fig. 5 shows the SEM micrographs of a graphite bar modified with the AuNPs-cys-glu-AuPDNs to be compared with a graphite bare. In the micrograph, despite the heterogeneous graphite surface, it is possible to see the Au-PDNs in the surface, in which the gold nanoparticles are distinguishable.

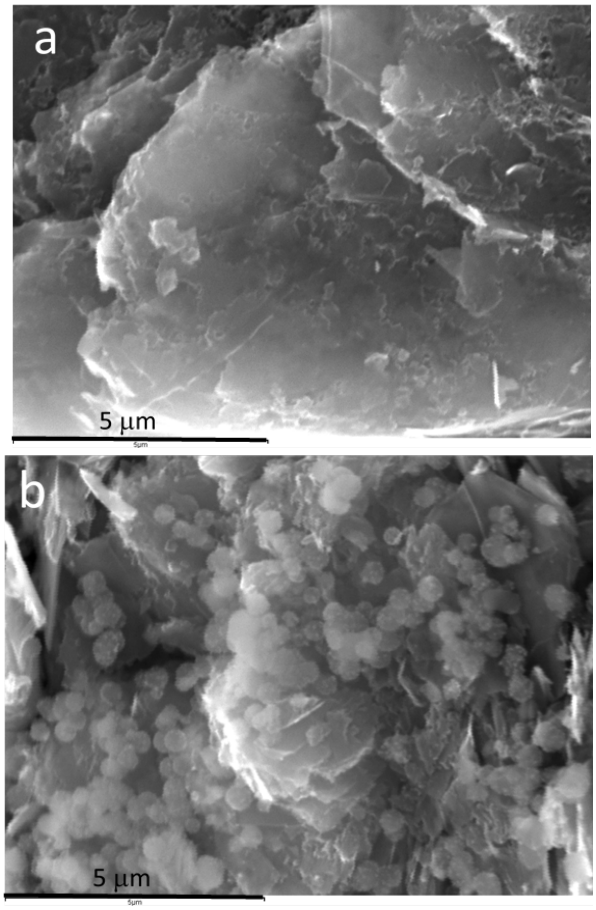

Fig. 5. SEM micrographs of a bare graphite bar (a) and the same modified with AuNPs-cys- glu-Au-PDNs SAM.

Usually, the properties of the electrode interface are studied also by EIS. The electrode interface can be modelled by an equivalent circuit that includes the charge-transfer resistance R_{CT} (electron transfer kinetics), the Warburg impedance (bulk-electrode interface ion diffusion), W, the double layer capacitance, C_{dl}, and the resistance of the solution, R_s. When the electrode surface is rough, C_{dl} may not correctly describe the electronic properties of the interface because the system move away from the ideal

capacitive behaviour [67]. For these surfaces, a constant phase element defined as $CPE = A^{-1}(j\omega)^{-N}$ that reflects the layer non-homogeneity, is introduced instead of C_{dl}, were N means the deviation of interface from the Randles model. The exponent N varies between 0.5 and 1 and A grows to be equal to C_{dl} when $N = 1$. The Nyquist plot consist of a semi-circular part al high frequencies, which diameter represents R_{CT}, and a linear part at low frequencies indicative of systems with diffusion-controlled current. Fig. 6 displays the Nyquist plots (impedance imaginary part vs. real part) obtained with all the unmodified and modified electrode types, and the Figs. S4, S5 and S6 shows the simulation fit with the obtained corresponding equivalent circuits.

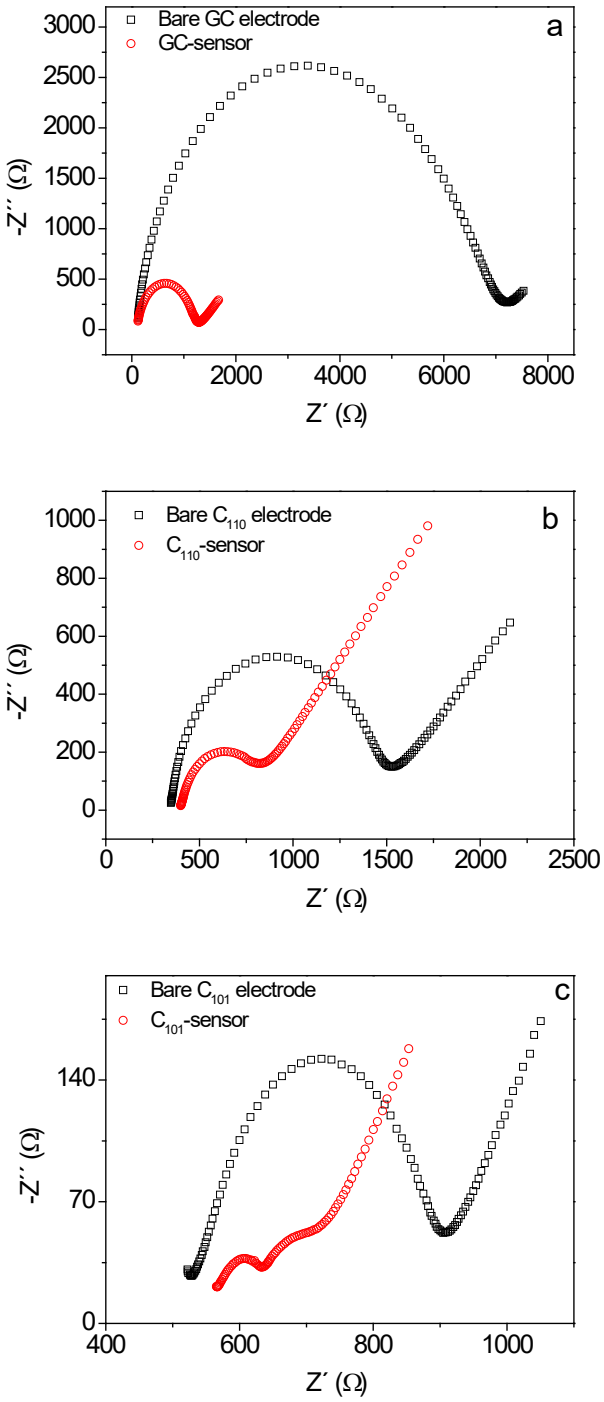

Fig. 6. Electrochemical impedance diagrams of the (a) GC-sensor and unmodified GC electrode, (b) C_{110}-sensor and unmodified C_{110} electrode, and (c) C_{101}-sensor and unmodified C_{101} electrode in a $K_3Fe(CN)_6/K_4Fe(CN)_6$ solution.

As it can be seen, the interfacial resistance of all the modified electrodes are significantly lower than those obtained for the corresponding bare electrodes, indicating high electrode-electrolyte electron conduction pathway in all the cases. Note the different shape of Nyquist plot of C_{101}-sensor, indicative of more irregular surface. The kinetic parameters i_0 (exchange current) and k^0 (the electron-transfer rate constant) can also be obtained from the impedance measurements [68], by the equations $R_{CT} = RT/nFi_0$, and $i_0 = nFAk^0C$, being C the concentration of the electroactive specie in mol cm^{-3} and A the electrode area in cm^2. Table 1 contains the results of all the electrochemical semi-circle fits (by the conventional Randles circuit) and the kinetic calculations. These results show that the charge transfer process of the $Fe(CN)_6^{4-/3-}$ redox system was improved in all the sensors in comparison with the bare electrodes.

Table 1
IES results from the electrochemical semi-circle fit

Electrode	R_{CT} (Ω)	*CPE* (μF)	*N*	i_0 (μA)	k^0 (cm s^{-1})
Bare GC	6937.3	0.211	0.9969	3.70	5.37×10^{-5}
GC-sensor	1135.9	0.242	0.9976	22.63	3.35×10^{-4}
Bare C_{110}	1131.9	1.001	0.9993	22.71	3.36×10^{-4}
C_{110}-sensor	483.9	2.744	0.9981	53.11	7.86×10^{-4}
Bare C_{101}	389.6	5.083	0.9972	65.97	9.76×10^{-4}
C_{101}-sensor (first semicircle)	108.6	3.230	0.9959	236.65	3.50×10^{-3}

3.3. Electrochemical behaviour of AA, DA, UA and TR at the modified electrodes

In order to investigate the reliability of the developed sensors, the electrocatalytic response of the GC-, C_{110}- and C_{101}-sensors toward the oxidation of AA, DA, UA and TR was investigated by differential pulse voltammetry (DPV) as sensitive and high-resolution technique. The physiological *pH* value, and therefore the most used, is 7.0. However, some authors have preferred other pH values due to the effect caused on the peak potentials and resolution of them. The reactions of oxidation of AA, DA, UA and TR (Fig.S7) involves a deprotonation step that is facilitated at higher *pH* values. This fact cause different shifts of peak potentials to more negative values depending on each corresponding *pKa* (AA: *pKa* = 4.10; DA: *pKa* = 8.87; UA: *pKa* = 5.7 and TR: *pKa* = 5.89) [69]. Fig. 7 shows the effect of *pH* value on the peak potential of the sensors developed with the three tested base-electrodes.

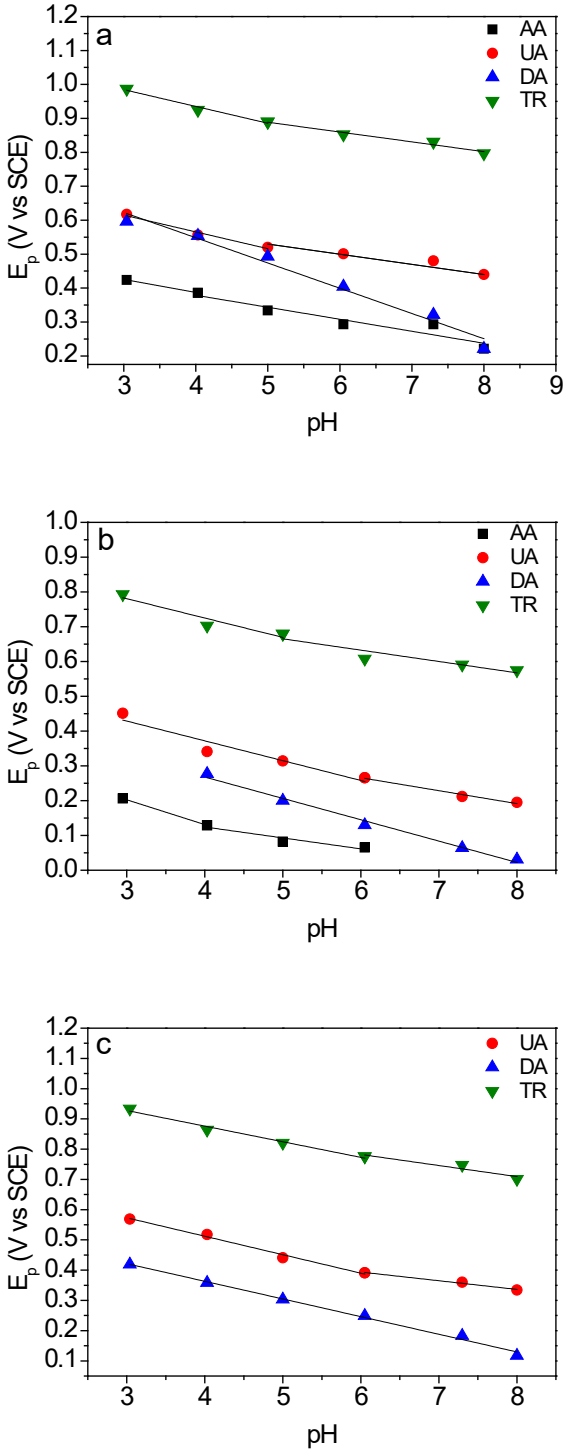

Fig. 7. Effect of *pH* on the peak potential for the oxidation of AA, DA, UA and TR (all 20 µM) at the GC- (a), C_{110}- (b) and C_{101}- (c) sensors in PBS.

As can be seen, in all the cases, linear fits with slopes (Table S1) close to 0.05916 (RT/F) were obtained, for *pH* values below the corresponding pKa values. As it was expected, slopes close to 0.02958 were obtained for higher pH values, indicating processes two proton – two electron for all the analytes(or one proton – two electron if pH > pKa). On the other hand, the analytes' peak currents, i_p, change notably with the pH

(Fig. S8) and these different sensitivities must be also considered in order to select the best conditions for the simultaneous determination. Both E_p and i_p vs *pH* plots confirm the C_{110} base electrode as the best because of the achieved sensitivity and peak resolution. This electrode, also offers the possibility of select the best *pH* value as a function of the sample composition or of their components concentrations' ranges. In the light of these results, we have selected the C_{110}-sensor and the *pH*-values of 3.0, 6.0 and 8.0 to study the simultaneous determination of AA, DA, UA and TR with the best sensitivity and selectivity.

3.4. Simultaneous determination of AA, DA, UA and TR

The simultaneous determination of AA, DA, UA and TR was carried out with differential pulse voltammetry (DPV) by the standard addition method. The analytes that did not show electrochemical signal were also included in the mixtures, with a concentration 1.0 mM. Figs. 8, 9 and 10 show the DPV of all the mixtures at 3.0, 6.0 and 8.0 *pH* values and the corresponding obtained calibration curves.

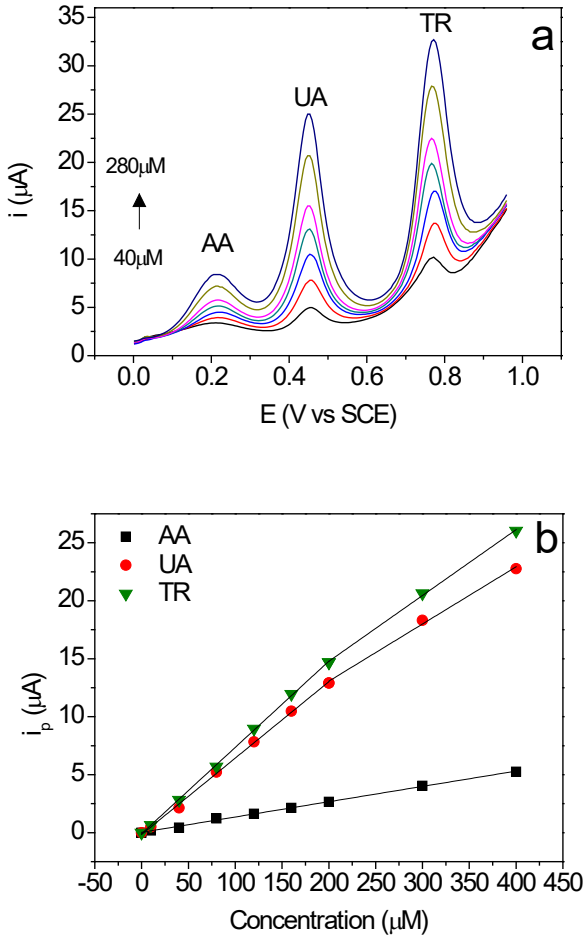

Fig. 8. DPVs measured at *pH* 3.0 in PBS containing 1 mM of DA and 40, 80, 120, 160, 200, 300, and 400 μM of each AA, UA and TR (a). Calibration curves for the same analytes and measuring conditions (b).

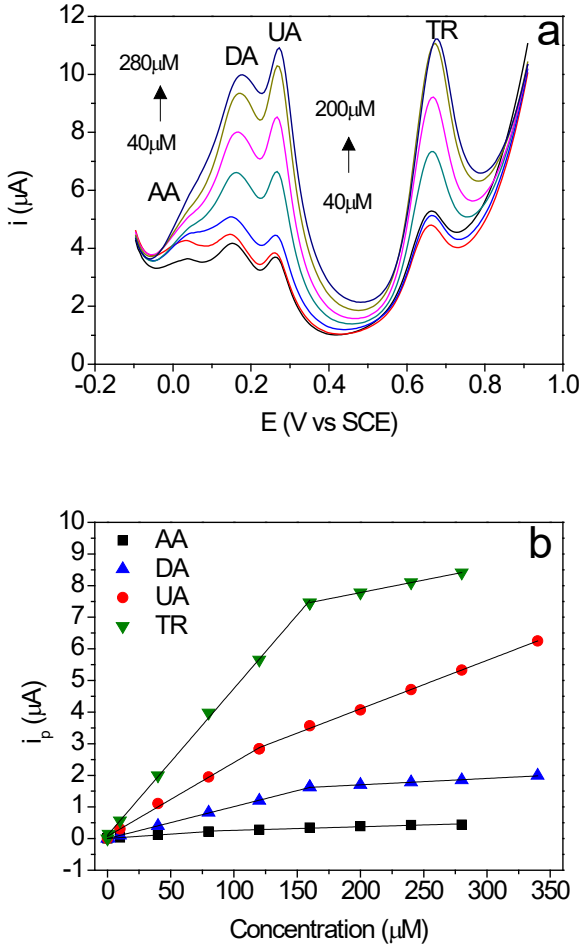

Fig. 9. DPVs measured at pH 6.0 in PBS containing 40μM of each analyte (first DPV), subsequent additions of 80, 120 μM AA (subsequent two DPVs), and subsequent simultaneous additions of 160, 200, 240, and 280 μM AA and 80, 120, 160 and 200 of each DA, UA and TR (subsequent four DPVs) (a). Calibration curves for the same analytes and measuring conditions (b).

As can be seen, AA, DA, UA and TR can be simultaneously determined at *pH* 6.0, and all of them show two linear ranges. At *pH* 3.0, AA, UA and TR can be determined without the DA interference. At *pH* 8.0, DA exhibits the best signal and can be determined together with UA and TR without the AA interference. The obtained sensitivities and detection limits, evaluated as three folds of the signal-to-noise ratio, are showed in Table 2. In addition, Table S2 shows the linear fits of *ip* vs concentration plots for the C_{110} sensor (average of five electrodes). These data demonstrate that this new development constitutes an interesting proposal to simultaneous determination of AA, DA, UA and TR, improving other recent published sensors, as the Table 3 demonstrates.

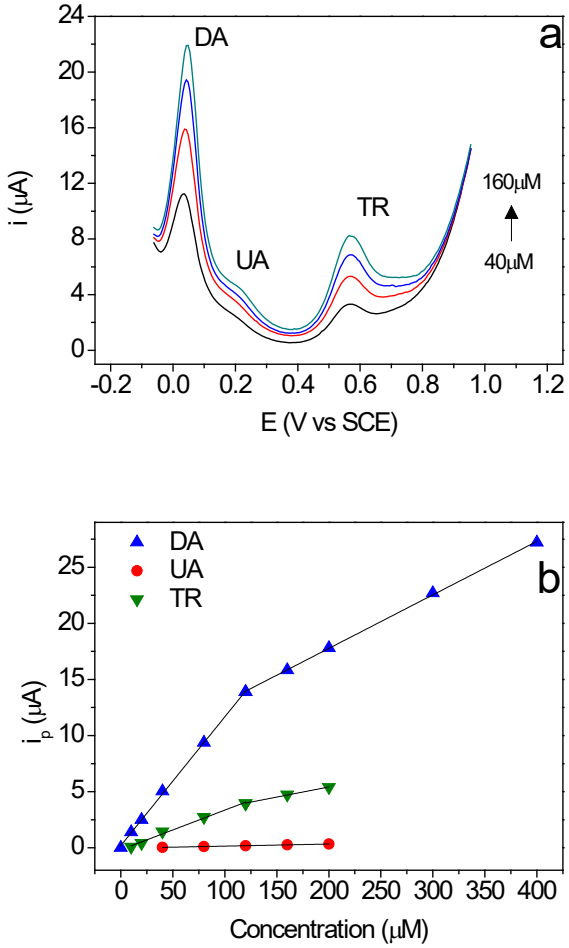

Fig. 10. DPVs obtained at pH 8.0 in PBS containing 1 mM of AA and 40, 80, 120 and 160 µM of each DA, UA and TR (a). Calibration curves for the same analytes and measuring conditions (b).

3.5. Interferences, repeatability and stability

To evaluate the selectivity of C_{110} sensor, the potential interferences of folic acid, glucose and several amino acids as alanine, glycine, glutamic acid, cysteine, valine and methionine were investigated. None of these compounds exhibit significant interference on the determination at the working *pH* values. Unlike other reported sensors, none adsorption was appreciated with the developed electrodes with any of studied analytes, and all the prepared electrodes were reused after wash them with deionized water without loss of activity or sensitivity. The stability was tested after a storage of two months and decreases lower than 1.8 % were observed for all the DPV signals. In continuous measurements, the electrodes have been used during 70 work hours and 200 measurements without any loss of signal. The electrode-to-electrode repeatability of the new sensor was carried out by DPV measurements of a mixture of AA, DA, UA and TR, all in concentration 60 µM at the three *pH* values, with five different electrodes. The obtained relative standard deviations are showed in the Table S2. All these results confirm that the new C_{110}-sensor exhibits very interesting stability and robustness properties.

Table 2
Analytical results for the C_{110} sensor. Average of five electrodes

pH	Analyte	Linear range (μM)	Sensitivity (μA μM^{-1} cm^{-2})	Detection Limit (nM)
3.00	AA	1 – 400*	0.105	0.1
	UA	1 – 200	0.524	0.1
		200 – 400*	0.392	
	TR	1 – 200	0.592	0.1
		200 – 400*	0.452	
6.00	AA	10 – 80	0.022	0.2
		80 – 240	0.011	
	DA	1 – 160	0.008	0.1
		160 – 350	0.016	
	UA	10 – 120	0.186	0.1
		120 – 350	0.123	
	TR	1 – 160	0.370	0.1
		160 - 280	0.063	
8.00	DA	1 – 120	0.914	0.1
		120 – 400*	0.380	
	UA	40 – 200*	0.015	40
	TR	1 – 120	0.261	0.1
		120 – 200*	0.143	

***** At least up to this value

4. Conclusions

A new electrochemical sensor based on a screen-printed carbon electrode covalently modified with self-assembled polydopamine nanospheres functionalized with gold nanoparticles has been developed. In order to select the best electrode-basis, a reusable GCE and two screen-printed electrodes (laminar and nanostructured) have been tested. The best performance was obtained with the C_{110}-sensor. All the modified electrodes have been characterized morphologically and electrochemically. The EIS study results show that the charge transfer process is improved in all the sensors in comparison with the bare electrodes. The best conditions for the simultaneous determination of these biomolecules can adapt to the characteristics of each sample (concentration and presence of analytes), being the 3.0, 6.0 and 8.0 the three *pH* values that let us achieve the best peak resolution. The simultaneous determination of AA, DA, UA and TR was possible at *pH* 6.0, in the linear ranges of 10 – 80 μM and 80 – 240 μM (AA); 1 – 160 μM and 160 – 350 μM (DA); 10 – 120 μM and 120 – 350 μM (UA); and 1 – 160 μM and 160 – 280 μM (TR) respectively. The obtained limits of detection were 0.2 nM, 0.1 nM, 0.1 nM and 0.1 nM, respectively. In addition, at *pH* 3.0, is possible to determine AA, UA and TR simultaneously in presence of DA, in more extended linear ranges and increased sensitivity. At *pH* 8.0, DA, UA and TR can be determined simultaneously, in presence of AA, also in more extended linear ranges and notably increased DA signal. Finally, the new C_{110}-sensor shows absence of poisoning failure and high stability and reproducibility, which makes it an interesting device to clinical and analytical applications.

Table 3
Comparison of the analytical characteristics of other different reported developments

Electrode	Analyte	Linear range (μM)	Detection limit (μM)	Sensitivity (μA μM^{-1} cm^{-2})	References
AgNC@PDA-NS/CFG/GCE	DA	2.5-130	0.25	0.538	[29]
	UA	10-130	1.9	0.156	
	AA	50-4000	6.4	0.0084	
Pt/IMo_6/GO-GCE	DA	4-750	0.22	0.0544	[70]
	UA	75-300	0.72	0.1457	
	AA	0.4-110	0.54	0.48[a]	
RGO-poly(PR)/AuNPs/GC	DA	0.4-170	0.005	0.40[a]	[71]
	UA	0.4-150	0.005	0.63[a]	
	AA	100-1000	39	0.0124	
GO/$TmPO_4$/GCE	DA	2-20	0.785	0.615	[72]
	UA	10-100	3.73	0.130	
	AA	0.06-100	0.4	0.239	
FOD/GCE	DA	0.06-50	0.2	0.460	[15]
	UA	0.06-100	0.2	0.453	
	TR	0.06-100	0.01	0.667	
PBDCNPE[b]	AA	1-80	0.3	0.143	[73]
	UA	-	-	0.0381	
	TR	-	-	0.0911	

Acknowledgments
The authors thank the Universidad Politécnica de Madrid for financial support of this research. The authors also thank the ICTS Centro Nacional de Microscopia Electrónica de la Universidad Complutense de Madrid for assistance in the SEM and TEM studies.

References

[1] O. Traxer, B. Huet, J. Poindexter, C. Y. C. Pak, M. S. Pearle, Effect of ascorbic acid consumption on urinary stone risk factors, J. Urol. 170 (2 P1) (2003) 397-401, https://doi.org/10.1097/01.ju.0000076001.21606.53.
[2] S. J. Padayatty, A. Katz, Y. Wang, P. Eck, O. Kwon, J. H. Lee, S. Chen, C. Corpe, A. Dutta, S. K. Dutta, M. Levine, Vitamin C as an Antioxidant: evaluation of its role in disease prevention, J. Am. Coll. Nutr. 22 (2003) 18-35, https://doi.org/10.1080/07315724.2003.10719272.
[3] T. R. Mikuls., C. H. MacLean, J. Olivieri, F. Patino, J. J. Allison, J. T. Farrar, W. B. Bilker, K. G. Saag, Quality of care indicators for gout management, Arthritis Rheum. 50 (3) (2004) 937–943, https://doi.org/10.1002/art.20102.
[4] B. F. Becker, Towards the physiological function of uric acid, Free Radic. Biol. Med. 14 (6) (1993) 615-631, https://doi.org/10.1016/0891-5849(93)90143-I.

[5] T. E. Smith, Molecular Cell Biology, in T. M. Devlin (editor), Textbook of Biochemistry with clinical Correlations, pp. 929, Wiley-Liss, New York (1999) ISBN: 978-0-470-28173-4.
[6] S. Kapur, R. Zipursky, C. Jones, G. Remington, S. Houle, Relationship between dopamine D2 occupancy, clinical response, and side effects: a double-blind pet study of first-episode schizophrenia, Am. J. Psychiatry 157 (2000) 514-520, https://doi.org/10.1208/s12248-010-9247-4.
[7] W. Kochen, H. Steinhart (Eds.), L-tryptophan: current prospects in medicine and drug safety, de Gruyter, Berlin (1994) ISBN: 3110136732.
[8] V. J. Knott, A. L. Howson, M. Perugini, A. V. Ravindran, S. N. Young, The effect of acute tryptophan depletion and fenfluramine on quantitative EEG and mood in healthy male subjects, Biol. Psychiatry 46 (1999) 229–238, https://doi.org/10.1016/S0006-3223(98)00338-2.
[9] E. Polo, S. Kruss, Nanosensors for neurotransmitters, Anal. Bioanal. Chem. 408 (2016) 2727-2741, https://doi.org/10.1007/s00216-015-9160-x.
[10] K. E. Hubbard, A. Wells, T. S. Owens, M. Tagen, C. H. Fraga, C. F. Stewart, Determination of dopamine, serotonin, and their metabolites in pediatric cerebrospinal fluid by isocratic high performance liquid chromatography coupled with electrochemical detection, Biomed. Chromatogr. 24 (6) (2010) 626-631, https://doi.org/10.1002/bmc.1338.
[11] S. Qi, B. Zhao, H. Tang, X. Jiang, Determination of ascorbic acid, dopamine, and uric acid by a novel electrochemical sensor based on pristine graphene, Electrochim. Acta 161 (2015) 395-402, https://doi.org/10.1016/j.electacta.2015.02.116.
[12] H. Karimi-Maleh, O. A. Arotiba, Simultaneous determination of cholesterol, ascorbic acid and uric acid as three essential biological compounds at a carbon paste electrode modified with copper oxide decorated reduced graphene oxide nanocomposite and ionic liquid, J. Coll. Inter. Sci. 560 (2020) 208-212, https://doi.org/10.1016/j.jcis.2019.10.007.
[13] E. A. Khudaish, K. Y. Al-Ajmi, S. H. Al-Harthi, A solid-state sensor based on ruthenium (II) complex inmobilized on polytyramine film for the simultaneous determination of dopamine, ascorbic acid and uric acid, Thin Solid Films 564 (2014) 390-396, https://doi.org/10.1016/j.tsf.2014.05.056.
[14] M. Taei, F. Hasanpour, N. Tavakkoli, M. Bahrameian, Electrochemical characterization of poly(fuchsine acid) modified glassy carbon electrode and its application for simultaneous determination of ascorbic acid, epinephrine and uric acid, J. Mol. Liq. 211 (2015) 353-36, https://doi.org/10.1016/j.molliq.2015.07.029.
[15] L. Fernández, M. Herrero, B. Alonso, C. M. Casado, M. P. García Armada, Three-dimensional electrocatalytic surface based on an octasilsesquioxane dendrimer for sensing applications, J. Electroanal. Chem. 839 (2019) 16–24, https://doi.org/10.1016/j.jelechem.2019.03.010.
[16] M. L. Yola, N. Atar, Functionalized graphene quantum dots with bi-metallic nanoparticles composite: Sensor application for simultaneous determination of ascorbic acid, dopamine, uric acid and tryptophan, J. Electrochem. Soc. 163 (2016) B718-B725, https://doi.org/10.1149/2.1191614jes.
[17] Y. Chen, X. F. Zhang, A. J. Wang, Q. L. Zhang. H. Huang, J. J. Feng, Ultrafine Fe3C nanoparticles embedded in N-doped graphitic carbon sheets for simultaneous determination of ascorbic acid, dopamine, uric acid and xanthine, Microchim. Acta 186 (2019) 660, https://doi.org/10.1007/s00604-019-3769-y.
[18] L. X. Chen, J. N. Zheng, A. J. Wang, L. J. Wu, J. R. Chen, J. J. Feng, Facile synthesis of porous bimetallic alloyed PdAg nanoflowers supported on reduced

graphene oxide for simultaneous detection of ascorbic acid, dopamine, and uric acid, Analyst, 2015,140, 3183-3192, https://doi.org/10.1039/C4AN02200A.
[19] T. Q. Xu, Q. L. Zhang, J. N. Zheng, Z. Y. Lv, J. Wei, A. J. Wang, J. J. Feng, Simultaneous determination of dopamine and uric acid in the presence of ascorbic acid using Pt nanoparticles supported on reduced graphene oxide, Electrochim. Acta 115 (2014) 109–115, http://dx.doi.org/10.1016/j.electacta.2013.10.147.
[20] E. Haghshenas, T. Madrakian, A. Afkhami, Electrochemically oxidized multiwalled carbon nanotube/glassy carbon electrode as a probe for simultaneous determination of dopamine and doxorubicin in biological samples, Anal. Bioanal. Chem. 408 (2016) 2577-2586, https://doi.org/10.1007/s00216-016-9361-y.
[21] F. Khaleghi, Z. Ara, V. K. Gupta, M. R. Ganjali, P. Norouzi, N. Atar, M. L. Yola, Fabrication of novel electrochemical sensor for determination of vitamin C in the presence of vitamin B9in food and pharmaceutical samples, J. Mol. Liq. 221 (2016) 666-672, http://dx.doi.org/10.1016/j.molliq.2016.06.061.
[22] M. Baghayeri, M. Nodehi, V. Heisi, M. B. Tehrani, B. Maleki, M. Mehmandost, The role of pramipexole functionalized MWCNTs to the fabrication of Pd nanoparticles modified GCE for electrochemical detection of dopamine, DARU J. Pharm. Sci. (2019). https://doi.org/10.1007/s40199-019-00287-y.
[23] C. Wang, J. Du, H. Wang, C. Zou, F. Jiang, P. Yang, Y. Du, A facile electrochemical sensor based on reduced graphene oxide and Au nanoplates modified glassy carbon electrode for simultaneous detection of ascorbic acid, dopamine and uric acid, Sensor. Actuator. B 204 (2014) 302-309, https://doi.org/10.1016/j.snb.2014.07.077.
[24] O. A. Yokuş, F. Kardaş, O. Akyıldırım, T. Eren, N. Atar, M. L. Yola, Sensitive voltammetric sensor based on polyoxometalate/reduced graphene oxide nanomaterial: Application to the simultaneous determination of l-tyrosine and l-tryptophan, Sensor. Actuator. B-Chem 233 (2016) 47-54, http://dx.doi.org/10.1016/j.snb.2016.04.050.
[25] H. Li, Y. Wang, D. Ye, J. Luo, B. Su, S. Zhang, J. Kong, An electrochemical sensor for simultaneous determination of ascorbic acid, dopamine, uric acid and tryptophan based on MWNTs bridged mesocellular graphene foam nano composite, Talanta 127 (2014) 255-261, https://doi.org/10.1016/j.talanta.2014.03.034.
[26] S. I. Kaya, S. Kurbanoglu, S. A. Ozkan, Nanomaterials-based nanosensors for the simultaneous electrochemical determination of biologically important compounds: ascorbic acid, uric acid, and dopamine, Crit. Rev. Anal. Chem. 49 (2019) 101-125, https://doi.org/10.1080/10408347.2018.1489217.
[27] M. E. Lynge, R. Van der Westen, A. Postma, B. Städler, Polydopamine a nature inspired polymer coating for biomedical science, Nanoscale 3 (2011) 4916-4928, https://doi.org/10.1039/C1NR10969C.
[28] X. Liu, X. Y. Zhang, L. L. Wang, Y. Y. Wang, A sensitive electrochemical sensor for paracetamol based on a glassy carbon electrode modified with multiwalled carbon nanotubes and dopamine nanospheres functionalized with gold nanoparticles, Microchim. Acta 181 (2014) 1439–1446, https://doi.org/10.1007/s00604-014-1289-3.
[29] Y. Li, Y. Jiang, Y. Song, Y. Li, S. Li, Simultaneous determination of dopamine and uric acid in the presence of ascorbic acid using a gold electrode modified with carboxilated graphene and silver nanocube functionalized polydopamine nanospheres, Microchim. Acta 185 (2018) 382, https://doi.org/10.1007/s00604-018-2922-3.

[30] X. Yao, C. Zhao, J. Kong, D. Zhou, X. Lu, Polydopamine-assisted synthesis of hollow $NiCo_2O_4$ nanospheres as high-performance lithium ion battery anodes, RSC Adv. 4 (2014) 37928-37933, https://doi.org/10.1039/C4RA06816E.
[31] E. Herlinger, R. F. Jameson, W. Linert, Spontaneous autoxidation of dopamine, J. Chem. Soc. Perkin. Trans. 2 (1995) 259-263, https://doi.org/10.1039/P29950000259.
[32] K. Y. Ju, Y. Lee, S. Lee, S. B. Park, J. K. Lee, Bioinspired polymerization of dopamine to generate melanin-like nanoparticles having an excellent free-radical-scavenging property, Biomacromolecules 12 (2011) 625-362, https://doi.org/10.1021/bm101281b.
[33] M. D'Ischia, A. Napolitano, V. Ball, C. T. Chen, M. J. Buehler, Polydopamine and eumelanin: from structure–property relationships to a unified tailoring strategy, Acc. Chem. Res. 47 (2014) 3541–3550, https://doi.org/10.1021/ar500273y.
[34] S. Cho, S. H. Kim, Hydroxide ion-mediated synthesis of monodisperse dopamine-melanin nanospheres, J. Colloid. Interf. Sci. 458 (2015) 87-93, https://doi.org/10.1016/j.jcis.2015.06.051.
[35] S. Xiong, Y. Wang, J. Yu, L. Chen, J. Zhu, Z. Hu, Polydopamine particles for next-generation multifunctional biocomposites, J. Mater. Chem. A 2 (2014) 7578-7587, https://doi.org/10.1039/C4TA00235K.
[36] Y. Liu, K. Ai, J. Liu, M. Deng, Y. He, L. Lu, Dopamine-melanin colloidal nanospheres: an efficient near-infrared photothermal therapeutic agent for in vivo cancer therapy, Adv. Mater. 25 (2013) 1353–1359, https://doi.org/10.1002/adma.201204683.
[37] J. Cui, Y. Yan, G. J. Such, K. Liang, C. J. Ochs, A. Postma, F. Caruso, Immobilization and intracellular delivery of an anticancer drug using mussel-inspired polydopamine capsules, Biomacromolecules 13 (8) (2012) 2225–2228, https://doi.org/10.1021/bm300835r.
[38] C. C. Ho, S. J. Ding, The pH-controlled nanoparticles size of polydopamine for anti-cancer drug delivery, J. Mater. Sci. Mater. Med. 24 (2013) 2381-2390, https://doi.org/10.1007/s10856-013-4994-2.
[39] Y. Li, Y. Jiang, T. Mo, H. Zhou, Y. Li, S. Li, Highly selective dopamine sensor based on graphene quantum dots self-assembled monolayers modified electrode, J. Electroanal. Chem. 767 (2016) 84–90, https://doi.org/10.1016/j.jelechem.2016.02.016.
[40] R. Liu, Y. Guo, G. Odusote, F. Qu, R. D. Priestley, Core-shell Fe_3O_4 polydopamine nanoparticles serve multipurpose as drug carrier, catalyst support and carbon adsorbent, Appl. Mater. Interfaces 5 (2013) 9167-9171, https://doi.org/10.1021/am402585y.
[41] D. Zhang, M. Wu, Y. Zeng, L. Wu, Q. Wang, X. Han, X. Liu, J. Liu, Chlorin e6 conjugated poly(dopamine) nanospheres as pdt/ptt dual-modal therapeutic agents for enhanced cancer therapy, Appl. Mater. Interfaces 7 (2015) 8176–8187, https://doi.org/10.1021/acsami.5b01027.
[42] Y. Dong, J. Cao, Y. Liu, S. Ma, A novel immunosensing platform for highly sensitive prostate specific antigen detection based on dual-quenching of photocurrent from CdSe sensitized TiO_2 electrode by gold nanoparticles decorated polydopamine nanospheres, Biosens. Bioelectron. 91 (2017) 246–252. https://doi.org/10.1016/j.bios.2016.12.043.
[43] S. Scarano, E. Pascale, P. Palladino, E. Fratini, M. Minunni, Determination of fermentable sugars in beer wort by gold nanoparticles@polydopamine: A layer-by-layer approach for localized surface plasmon resonance measurements at fixed

wavelength, Talanta, 183 (2018) 24-32, https://doi.org/10.1016/j.talanta.2018.02.044.
[44] T. Zeng, X. Zhang, H. Niu, Y. Ma, W. Li, Y. Cai, In situ growth of gold nanoparticles onto polydopamine-encapsulated magnetic microspheres for catalytic reduction of nitrobenzene, App. Catal. B Environ. 134–135 (2013) 26–33, http://dx.doi.org/10.1016/j.apcatb.2012.12.037.
[45] Y. Zhao, Y. Yeh, R. Liu, J. You, F. Qu, Facile deposition of gold nanoparticles on core-shell Fe_3O_4@polydopamine as recyclable nanocatalyst, Solid State Sci. 45 (2015) 9-14, https://doi.org/10.1016/j.solidstatesciences.2015.04.010.
[46] N. Rahoui, B. Jianga, M. Hegazy, N. Taloub, Y. Wang, M.Yu, Y. D. Huang, Gold modified polydopamine coated mesoporous silica nano-structures for synergetic chemo-photothermal effect, Colloid. Surface. B 171 (2018) 176-185, https://doi.org/10.1016/j.colsurfb.2018.07.015.
[47] S. J. Lee, H. Lee, S. Kim, J. M. Seok, J. H. Lee, W. D. Kim, I. K. Kwon, S. Park, S. A. Park, In situ gold nanoparticle growth on polydopamine-coated 3D-printed scaffolds improves osteogenic differentiation for bone tissue engineering applications: in vitro and in vivo studies, Nanoscale 10 (2018) 15447-15453, https://doi.org/10.1039/C8NR04037K.
[48] X. Xu, Q. Zheng, G. Bai, L. Song, Y. Yao, X. Cao, S. Liu, C. Yao, Polydopamine induced in-situ growth of Au nanoparticles on reduced graphene oxide as an efficient biosensing platform for ultrasensitive detection of bisphenol A, Electrochim. Acta 242 (2017) 56-65 https://doi.org/10.1016/j.electacta.2017.05.007.
[49] Y. Wang, Y. Xiong, J. Qu, J. Qu, S. Li, Selective sensing of hydroquinone and catechol based on multiwalled carbon nanotubes/polydopamine/gold nanoparticles composites, Sensor. Actuat. B-Chem. 223 (2016) 501-508, https://doi.org/10.1016/j.snb.2015.09.117.
[50] J. Zhang, L. Mou, X. Jiang, Hydrogels Incorporating Au@Polydopamine Nanoparticles: Robust Performance for Optical Sensing, Anal. Chem. 90 (2018) 11423−11430, https://doi.org/10.1021/acs.analchem.8b02459.
[51] N. Atar, T. Eren, M. L. Yola, Ultrahigh capacity anode material for lithium ion battery based on rod gold nanoparticles decorated reduced graphene oxide, Thin Solid Films, 590 (2015) 156–162, https://doi.org/10.1016/j.tsf.2015.07.075.
[52] M. L. Yola, N. Atar, Z. Üstündag, A. O. Solak, A novel voltammetric sensor based on p-aminothiophenol functionalized graphene oxide/gold nanoparticles for determining quercetin in the presence of ascorbic acid, J. Electroanal. Chem. 698 (2013) 9-16, http://dx.doi.org/10.1016/j.jelechem.2013.03.016.
[53] V. K. Gupta, M. L. Yola, M. S. Qureshie, A. O. Solak, N. Atare, Z. Üstündag, A novel impedimetric biosensor based on graphene oxide/gold nanoplatform for detection of DNA arrays, Sensor. Actuator. B-Chem. 188 (2013) 1201–1211, http://dx.doi.org/10.1016/j.snb.2013.08.034.
[54] E. Ospina, C. M. Casado, B. Alonso, M. P. García Armada, Thiolated DAB dendrimers-gold nanoparticles as self-assembled layers for the direct electrochemistry of HRP, J. Electrochem. Soc. 166 (2019) B1434-B1440, http://doi.org/10.1149/2.0411915jes.
[55] L. Shi, Z. Wang, X. Chen, G. Yang, W. Liu, Reduced Graphene Oxide/Polydopamine/Gold Electrode as elecrochemical sensor for simultaneous determination of ascorbic acid, dopamine, and uric acid, Int. J. Electrochem. Sci. 14 (2019) 8882 – 8891, https://doi.org/10.20964/2019.09.49.
[56] G. Xua, J. Houb, Y. Zhao, J. Bao, M. Yang, H. Fa, Y. Yang, L. Li, D. Huo, C. Hou, Dual-signal aptamer sensor based on polydopamine-gold nanoparticles and

exonuclease I for ultrasensitive malathion detection, Sensor. Actuator B-Chem. 287 (2019) 428-436, https://doi.org/10.1016/j.snb.2019.01.113.
[57] E. Çevik, O. Bahar, M. Şenel, M. F. Abasıyanık, Construction of novel electrochemical immunosensor for detection of prostate specific antigen using ferrocene-PAMAM dendrimers, Biosens. Bioelectron. 86 (2016) 1074–1079, https://doi.org/10.1016/j.bios.2016.07.064.
[58] P. Bollella, F. Mazzei, G. Favero, G. Fusco, R. Ludwig, L. Gorton, R. Antiochi, Improved DET communication between cellobiose dehydrogenase and a gold electrode modified with a rigid self-assembled monolayer and green metal nanoparticles: The role of an ordered nanostructuration, Biosens. Bioelectron. 88 (2017) 196–203, https://doi.org/10.1016/j.bios.2016.08.027.
[59] A. Li, J. Zhang, J. Qiu, Z. Zhao, C. Wang, C. Zhao, H. Liu, A novel aptameric biosensor based on the self-assembled DNA–WS2 nanosheet architecture, Talanta 163 (2017) 78–84, https://doi.org/10.1016/j.talanta.2016.10.088.
[60] L. J. Lai, Y. W. Yang, Y. K. Lin, L. L. Huang, Y. H. Hsieh, Surface characterization of inmunosensor conjugated with gold nanoparticles based on cyclic voltammetry and X-ray photoelectron spectroscopy, Colloid. Surface. B 68 (2009) 130-135, https://doi.org/10.1016/j.colsurfb.2008.09.010.
[61] R. K. Shervedani, M. Bagherzadeh, S. A. Mozaffari, Determination of dopamine in the presence of high concentration of ascorbic acid by using gold cysteamine self-assembled monolayers as a nanosensor, Sensor. Actuator. B-Chem. 115 (2006) 614-621, https://doi.org/10.1016/j.snb.2005.10.027.
[62] Y. Xue, X. Li, H. Li, W. Zhang, Quantifying thiol-gold interactions towards the efficient strength control, Nat. Commun. 5 (2014) 4384, https://doi.org/10.1038/ncomms5348.
[63] R. Sharma, R. K. Sinha, V. V. Agrawal, Mediator-free total cholesterol estimation using a bi-enzyme functionalized nanostructured gold electrode, RSC Adv. 5 (2015) 41786-41794, https://doi.org/10.1039/C5RA03053F.
[64] I. El-Hallag, A. O. Al-Youbi, A. Y. Obaid, E. H. El-Mossalamy, S. A. El-Daly, A. M. Asiri, Electrochemical Investigation of cysteamine at carbon fiber microdisk electrode, J. Chil. Chem. Soc. 56 (2011) 837-841, http://dx.doi.org/10.4067/S0717-97072011000400003.
[65] J. Wang, Analytical Electrochemistry, third ed. pp 32, John Wiley & Sons, Inc, New York (2006) ISBN-13 978-0-471-67879-3.
[66] A. A. Abdelwahab, Y. B. Shim, Simultaneous determination of ascorbic acid, dopamine, uric acid and folic acid based on activated graphene/MWCNT nanocomposite loaded Au nanoclusters, Sensor. Actuator. B 221 (2015) 659-665, https://doi.org/10.1016/j.snb.2015.07.016.
[67] E. Katz, I. Willner, Probing biomolecular interactions at conductive and semiconductive surfaces by impedance spectroscopy: routes to impedimetric immunosensors, DNA-sensors, and enzyme biosensors, Electroanalysis, 15 (2003) 913–947, https://doi.org/10.1002/elan.200390114.
[68] A. J. Bard, L. R. Faulkner, Electrochemical Methods. Fundamentals and Applications, second ed. pp. 381, John Wiley & Sons, Inc. New York (2001) ISBN 0-471-04372-9.
[69] C. Wang, R. Yuan, Y. Chai, S. Chen, F. Hu, M. Zhang, Simultaneous determination of ascorbic acid, dopamine, uric acid and tryptophan on gold nanoparticles/overoxidized-polyimidazole composite modified glassy carbon electrode, Anal. Chim. Acta 741 (2012) 15-20, https://doi.org/10.1016/j.aca.2012.06.045.

[70] L. Zhang, J. Khungwa, Y. Liu, L. Li, X. Wang, S. Wang, Fabrication of electro-active Pt/IMo6O24/graphene oxide nanohybrid modified electrode for the simultaneous determination of ascorbic acid, dopamine and uric acid, J. Electrochem. Soc. 166 (2019) H351–H358, https://doi.org/10.1149/2.1141908jes.
[71] N. M. M. A. Edris, J. Abdullah, S. Kamaruzaman, Y. Sulaiman, Ultrasensitive reduced graphene oxide-poly(procion)/gold nanoparticles modified glassy carbon electrode for selective and simultaneous determination of ascorbic acid, dopamine, and uric acid, J. Electrochem. Soc. 166 (2019) B664–B672, https://doi.org/10.1149/2.0931908jes.
[72] H. Huang, Y. Yue, Z. Chen, Y. Chen, S. Wu, J. Liao, S. Liu, H. Wen, Electrochemical sensor based on a nanocomposite prepared from $TmPO_4$ and graphene oxide for simultaneous voltammetric detection of ascorbic acid, dopamine and uric acid, Microchim. Acta (2019) 186:189, https://doi.org/10.1007/s00604-019-3299-7.
[73] M. Mazloum-Ardakani, M. Abolhasani-Soorki, A. Khoshroo, F. Sabaghian, B. F. Mirjalili, Simultaneous determination of ascorbic acid, uric acid and tryptophan by novel carbon nanotube paste electrode, Iran. J. Pharm. Res. 17 (2018) 851-863, PMID: 30127810, PMCID: PMC6094440.